DOI: 10.1002/ ((please add manuscript number))
Full Paper

Gold Nanoparticles in DNA-Based Multilayer Films: Synthesis, Size Control, and Influence of the Multilayer Structure on Au NP Catalytic Properties

Anatoly Zinchenko, Chihiro Nagahama, Shizuaki Murata*

Dr. A. Zinchenko, C. Nagahama, Prof. S. Murata
Graduate School of Environmental Studies, Nagoya University, Furo-cho, Chikusa-ku, Nagoya, 464-8601, Japan
E-mail: zinchenko@urban.env.nagoya-u.ac.jp

Keywords: DNA, multilayers, thin films, nanoparticles, catalysis

Abstract A method to prepare DNA-based multilayered microcapsules as a host matrix for synthesis of ultrasmall gold nanoparticles of 2-4 nm size was elaborated. Utilizing the intrinsic affinity of DNA for transition metal ions, ionic gold was first efficiently concentrated inside the DNA-based multilayer assembled on a CaCO3 sacrificial template. Further reduction of ionic gold inside the multilayer resulted in formation of a high-density well dispersed of 2-4 nm gold nanoparticles distributed evenly and exclusively inside the polyelectrolyte multilayer. Metallized multilayers containing ultrafine gold nanoparticles showed a good performance in catalytic reduction of nitroaromatic compounds and the catalytic activity of gold nanoparticles was enhanced with a decrease of host multilayer thickness. The influence of the multilayer structure and composition on the catalytic activity of gold NP are discussed.

1. Introduction

Outstanding optical, electric, catalytic, magnetic, etc. properties of noble metal nanoparticles (NP) are well known and broadly utilized in various applications.[1] In these applications, stabilization of noble metal NP of several nanometer size is crucial to overcome the issues related to nanoparticles aggregation and chemical transformation; therefore, suitable techniques for NP stabilization are required to facilitate NP manipulation, collection, and reuse in areas of catalysis, bioimaging, sensors, etc.[2] Conventional methods for noble NP stabilization in solution generally rely on electrostatic or steric stabilization of NP by low-molecular-weight binders, polymers, etc. On the other hand, synthesis of nanoparticles in a suitable permeable polymeric matrices such as hydrogels[3] or polyelectrolyte (PE) multilayers[4] was shown to be an alternative strategy to maintain a high concentration of nanoparticles and, at the same time, to prevent nanoparticles' aggregation as a result of local fixation of NP on DNA matrix scaffolds.[5] Utilization of DNA macromolecules to construct matrices for noble NP preparation is particularly advantageous because DNA, having a remarkable affinity to most of known transition metals,[6] can function as an adsorbent and promote a substantial decrease of NP size as a result of faster nucleation of NP on DNA. In past decades, the application of DNA as an industrial material is increasingly considered due to availability of industrial scale low-cost DNA extracted from fish milt, the waste product of marine industry.[7]

Recently, we reported the construction of DNA-based "soft catalyst" containing gold NPs inside the matrix of DNA hydrogel and used it in a catalytic reaction.[3h, 8] Although DNA hydrogel was shown to be a good matrix for concentration of Au precursor and synthesis of catalytically active gold NP, further it became clear that due to poor

accessibility of gold NP for reactants and diffusion limitations inside hydrogel matrix the catalytic activity of NP embedded in the hybrid hydrogel was significantly lower than that of gold NP dispersions of the same amount.[8] To overcome these limitations, utilization of thin films as a templating platform for catalytic NP should be advantageous to facilitate the kinetics of reactants diffusion and, thus, increase the efficiency of catalysis. Construction of thin films from oppositely charged polyelectrolytes (PE) by layer-by-layer deposition (LbL) is a well-developed technique that was utilized to construct a broad variety of functional materials.[9] A great number of approaches to the construction of multilayers containing nanoparticles was reported, and most of them are based either on (i) diffusion of nanoparticles into already assembled multilayers, (ii) step-by-step deposition of polyelectrolytes and NP of opposite charges, or (iii) diffusion of cations or of metal complexes inside multilayer films and their subsequent reduction to NP. In the first and second methods a large excess of noble metal NP should be used during the construction of hybrid multilayers and NP size control in situ is not possible. In the third method, due to weak metal binding to PE in multilayers studied so far, reduction of metal precursor is difficult to control as it occurs both in multilayers and in solution. Therefore, design and construction of further more functional multilayers with embedded nanoparticles remains a challenge.

Herein, we elaborated a new functional multilayer system utilizing double-stranded DNA that can efficiently concentrate noble metal inside PE multilayer. The precise control of the amount of Au precursor absorbed by DNA inside the multilayer was used to produce well defined gold NP in the multilayer film with a size of 2-3 nanometers and a narrow size distribution. The catalytic properties of Au nanoparticles embedded in

PE layer were tested on a *p*-nitrophenol reduction model system under condition of varied thickness of multilayer and degree of multilayer saturation with gold to gain deeper understanding about the factors controlling catalytic properties of noble metal NP inside the PE multilayer.

2. Results and Discussion

2.1. Construction of polyelectrolyte capsules with embedded ultrasmall gold nanoparticles

The overall process used for construction of polyelectrolyte microcapsules and their subsequent metallization is shown in **Figure 1**. Oppositely charged polyelectrolytes, anionic double-stranded DNA and cationic poly(diallyldimethylammonium chloride) (PDADMAC), were used as building blocks for constriction of polyelectrolyte multilayers on $CaCO_3$ microbead templates (**Figure 1B**) according to standard layer-by-layer (LbL) deposition procedure.[9] DNA is characterized by high binding constants to most of transition metals,[5] and, thus, utilization of DNA as a component of PE multilayers is essentially important for efficient enrichment and entrapping of metal precursor inside multilayers (**Figure 1C**). DNA-bound metal ions are further reduced and converted to metal nanoparticles embedded inside the multilayers (**Figure 1D**). $CaCO_3$ beads can be optionally dissolved by EDTA solutions to obtain metallized PE microcapsules (**Figure 1E**).

Experimentally, $CaCO_3$ beads of 6.0±1.5 μm size were prepared by mixing 0.33 M solutions of Na_2CO_3 and $CaCl_2$ as reported earlier.[10] **Figures 2A,B** show typical light and fluorescent microscopy images of $CaCO_3$ beads labeled with Ca^{2+} specific fluorescent probe, calcein, emitting green fluorescent light. Freshly prepared $CaCO_3$

beads were used as templates for deposition of anionic DNA and cationic PDADMAC polyelectrolytes to assemble a polyelectrolyte multilayer film on a surface of beads. $CaCO_3$ beads are positively charged at neutral pH,[11] therefore, anionic DNA was deposited on a surface of $CaCO_3$ beads as the first layer. Next, layers of PDADMAC and DNA were sequentially deposited according to the standard LbL protocol.[10-11] In order to prevent penetration of DNA chains inside pores of calcium carbonate beads and to obtain stable polyelectrolyte network on a surface of the beads, long, *ca.* 20,000 bp DNA (*ca.* 6 μm contour length) was used for deposition of the first layer, but the other layers of DNA were assembled using a shorter 300 bp DNA to prevent aggregation of beads caused by cross-linking of multiple beads by single DNA chains. Using the LbL method, multilayers containing 3, 5, and 7 layers of polyelectrolytes were constructed and abbreviated hereafter as $(DNA)_2(PDADMAC)_1$, $(DNA)_3(PDADMAC)_2$, and $(DNA)_4(PDADMAC)_3$, respectively. The inner and the outer layers of thus prepared multilayers are made of DNA in order to provide higher negative charge resulted in a better electrostatic stability of the beads against aggregation.

The amount of deposited DNA on $CaCO_3$ beads was measured quantitatively from the change in UV absorbance of DNA (λ=260 nm) in the supernatant above beads before and after DNA deposition. **Figure 2C** shows that each step of DNA adsorption was characterized by the same amount of DNA deposited on the beads surface. Incorporation of DNA into the multilayer was visualized by fluorescent microscopy by labeling DNA with DAPI fluorescent dye (**Figure 2D)** and $CaCO_3$ core with calcein. All the observed beads had a bright blue fluorescent surface layer (DAPI) of evenly distributed intensity. The fluorescent images in **Figure 2D** also indicate that DNA did not penetrate inside the nanoporous beads in a good agreement with the earlier studies

demonstrated that polyelectrolyte chains about several thousand kDa (polymerization degree on the order of 10,000) do not penetrate through *ca.* 30 nm pores of the beads.[11]

Metallization of DNA, i.e. adsorption of metal precursor by DNA in the polyelectrolyte multilayer followed by its reduction (**Figure 1C,D**), can be performed either in the presence of $CaCO_3$ bead template or after its dissolution. Both procedures were tested in this study but it was found that removal of $CaCO_3$ template before metallization caused a stronger aggregation of hollow capsules during metallization process, although the spherical morphology of the capsules was preserved. Therefore, here we mainly describe the former construction procedure as the preferable method, according to which DNA-containing multilayer deposited on $CaCO_3$ template is metallized.

Beads with 3, 5, and 7 layers of polyelectrolytes, i.e. $(DNA)_2(PDADMAC)_1$, $(DNA)_3(PDADMAC)_2$, and $(DNA)_4(PDADMAC)_3$, were used as a host matrix for absorbance of $HAuCl_4$ precursor (**Figure 1C**) followed by its reduction to gold nanoparticles (**Figure 1D**). Aqueous $HAuCl_4$ represents a mixture of mono-anionic complexes $[AuCl_x(OH)_{4-x}]^-$ with the composition depending on solutions pH.[12] Coordination of DNA bases with gold complexes was suggested to occur after formation of cationic species $[AuCl_2]^+$ and subsequent formation of coordination bonds between Au and nitrogen atoms of DNA bases.[13] Electrostatic binding of $[AuCl_x(OH)_{4-x}]^-$ anions to non-compensated charges of he PDADMAC polycation might also take place, but because the charge of Au complex is only −1 and this interaction is not specific, such interaction with DNA would not contribute much to the uptake of Au ion by the multilayer. When beads with the PE multilayers were dispersed in solutions of $HAuCl_4$, the color of dispersions changed gradually from white to

yellow-brown (**Figure 3A, left**) and the color intensity of beads correlated well with the number of DNA layers. The kinetics of $HAuCl_4$ concentration decrease in solution above beads was measured by atomic absorption spectroscopy (AAS) (**Figure 3B**). The multilayers were saturated by $HAuCl_4$ within about an hour and the amount of adsorbed $HAuCl_4$ by beads with 3, 5, and 7 layers of polyelectrolytes depended on the amount of DNA in multilayers, but the average gold/DNA ratios were about 0.5-0.7.

After saturation of multilayers by gold precursor, beads were washed with Milli-Q water and the gold ions localized in the multilayers were reduced by adding freshly prepared solution of $NaBH_4$ (10 mM). Immediately after addition of the reducing agent the color of beads suspensions changed to intensively colored purple or violet dispersions indicating the formation of gold nanostructures in the multilayers (**Figure 3A (left)**). Spectroscopy and microscopy characterizations of gold nanostructures formed inside the polyelectrolyte multilayer was difficult in the presence of inorganic template, therefore, $CaCO_3$ cores were dissolved by adding 0.1 M EDTA solution (pH = 7.2) and further analyses were performed using the hollow capsules. After dissolution of $CaCO_3$ templates even capsules containing only 3 PE layers ($(DNA)_2(PDADMAC)_1$) remained stable and no spherical shape deformation was observed.

UV-Vis spectra of metallized multilayers are shown in **Figure 3C**. Absorbance in the visible range of spectrum indicates the presence of gold nanoparticles in the analyzed samples. The character of spectrum depended on the number of polyelectrolyte layers. The spectrum of metallized $(DNA)_2(PDADMAC)_1$ multilayer had clear characteristic plasmonic signal of gold nanostructures at around λ=520 nm. The spectrum of nanoparticles synthesized in $(DNA)_3(PDADMAC)_2$ broadened and shifted to longer wavelength with the maximum absorbance at *ca.* 650 nm. Further increase in the

number of layers in $(DNA)_4(PDADMAC)_3$ caused a furthermore remarkable broadening of spectrum and its red shift.

Figure 4 shows typical transmission electron microscopy images of metallized $(DNA)_3(PDADMAC)_2$ capsules containing gold nanostructures formed in multilayers. Metallized capsules are characterized by spherical morphology and meshed structure of the surface layer (**Figure 4A**). The magnified images in **Figure 4B,C** show that the multilayer of capsules incorporate a large number of small gold nanoparticles of a very high density that are evenly distributed over the whole area of the multilayer film and show a minimal aggregation/fusion. The elemental analysis of the metallized capsules' composition by energy dispersive X-ray spectroscopy (EDS) (**Figure 4D**) revealed the presence of both gold and phosphorous of DNA at approximately equal atomic concentrations, which is satisfactorily consistent with the amount of adsorbed gold by DNA in multilayers measured by AAS (**Figure 3B**).

The morphology and gold NP arrangement in the metallized multilayers observed by TEM was similar for all three types of capsules but sizes and surface densities of NP varied. Size distributions of gold nanoparticles in the multilayers containing 3, 5, and 7 layers of polyelectrolytes are shown in **Figure 5A-C** together with the dependences of NP average size on the number of DNA layers (**Figure 5D**). Increase in the number of DNA layers from 2 to 4 resulted in only a slight increase of gold nanoparticles size from 3.2±0.7 nm to 3.8±0.9 nm (**Figure 5D**).

To make clear the influence of the amount of adsorbed gold by DNA in the multilayers on the morphology and size of gold NP, metallization of multilayers containing lower concentrations of gold in respect to available DNA binding sites was also studied. The same amounts of beads were placed for 3 hours in solutions containing

varied concentrations of $HAuCl_4$ and multilayers containing gold ion of the quantity ranging from full saturation to *ca.* 40% of the maximum value were obtained. Metallization of capsules containing different amounts of adsorbed gold was performed using the same concentration of $NaBH_4$ (10 mM). The color of thus prepared metallized beads was similar, but the size and density of gold nanoparticles inside the multilayers visualized by TEM drastically changed. Comparison of **Figures 4C and 4D** indicates that the two main consequences of the decreased gold/DNA ratios were (i) smaller average size of gold nanoparticles and (ii) lower surface density in gold nanoparticles inside the multilayer (**Figure 4E**). **Figure 5E** shows the change in Au NP average size occurred as a result of a decrease of gold/DNA ratios. The values under experimental points show Au/P ratios measured by EDS. The average size of gold nanoparticles was reduced almost two-fold in comparison to saturated multilayer films and reached as small as 2 nm size.

The results of binding degrees of gold to DNA and the sizes of Au NP (**Figure 5E**) were used to calculate the average length of DNA corresponding to the number of Au atoms to form a single NP in each case. **Figure 6A** shows that the length of DNA template required for construction of one NP is independent on the degree of DNA template saturation and equals to about 400-500 nm. Based on these results, the proposed scenario of gold NPs growth on DNA template is illustrated by **Figure 6B**. It is suggested that the constancy of DNA length relates to the mobility of the reduced gold atoms along DNA template during NP growth. Mobility of Au clusters/NP is significantly slower than that of Au atoms, therefore, in the process of NP formation, atoms of Au move along DNA to combine with a growing cluster of Au. The distance between thus formed NP is determined by the kinetics of new clusters formation and the

kinetics of Au atoms diffusion along DNA chain. Provided that the nucleation speed and the mobility of Au atoms is not influenced by the saturation degree, higher binding degrees of Au to DNA favor the formation of larger NP (**Figure 6B**).

Utilizing DNA affinity to other transition metal, above metallization protocol is suitable to perform metallization of DNA-containing multilayers with nanoparticles of other metals. For example, Figure 4(D-F) shows TEM images of metallized capsules obtained by adsorption of $AgNO_3$ by $(DNA)_3(PDADMAC)_2$ and reduction by $NaBH_4$ under conditions the capsules were metallized by gold. Similarly to the metallization of multilayers by gold, the multilayers contained a large quantity well dispersed silver nanoparticles of 3.8±1.2 nm.

2.2. Catalytic activity of gold nanoparticles embedded in polyelectrolyte multilayer film

Multilayered capsules containing ultrasmall gold NP were next tested as catalysts in a model system – reduction of nitroaromatic compound. The analysis of catalytic activity of the metallized multilayers was performed in the presence of $CaCO_3$ beads. The same amount of $(DNA)_2(PDADMAC)_1$, $(DNA)_3(PDADMAC)_2$, and $(DNA)_4(PDADMAC)_3$ beads (10 μL of 2.5% solution) were added to an aqueous solution of *p*-nitrophenol (0.02 mM) and $NaBH_4$ (10 mM), and the conversion of *p*-nitrophenol to *p*-aminophenol was monitored spectroscopically as a change in UV absorbance of *p*-nitrophenol at λ=400 nm and *p*-aminophenol at λ=310 nm (**Figure 7A**). Spectroscopic data of *p*-nitrophenol catalytic reduction catalyzed by three types of beads are summarized in **Figure 7B** in the coordinates of first-order reaction kinetics, i.e. as the dependences of

$\ln\left(\frac{[A]}{[A]_0}\right)$ on the time of the reaction (t), where $[A]$ and $[A]_0$ are *p*-nitrophenol absorbances at time $t = t$ and at $t_0 = 0$, respectively. All the dependences obeyed the first-order reactions equation after initial delay ("induction time"), the region of kinetic curve with almost zero slope. This "incubation time" is a typical feature of the catalysis by NP embedded in polymer matrices and it is related to the surface restructuring of the nanoparticles before before the catalytic reaction starats.[3g, 3h-j] The apparent rate constants (k_{app}) of catalytic processes were calculated from the spectroscopic data and summarized in **Table 1**. The highest apparent rate constant k_{app} = 0.279 s^{-1} was found in catalysis by $(DNA)_2(PDADMAC)_1$ containing the minimal number of polyelectrolyte layers. Catalysis by capsules with 5 layers was of the similar efficiency (k_{app} = 0.240 s^{-1}). In contrast, despite of a larger number of gold NP incorporated in the multilayer of $(DNA)_4(PDADMAC)_3$, the reaction in the presence of the capsules containing 7 polyelectrolyte layers was significantly slower and characterized by about 3-fold decrease of rate constant (k_{app} = 0.058 s^{-1}). In literature, the catalytic activity of gold nanoparticles was shown to depend on their size[14] but a good linear correlation between the reaction rate constant and the total surface area of gold NP was reported.[15] To address the difference in the total surface area of gold NP used in for catalysis, **Table 1** shows the data of recalculated rate constants ($k_1 = k_{app}/S$) normalized by surface area (S) of gold NP. Even after normalization it is obvious that the catalysis by beads with 3-layers of polyelectrolytes was the most efficient, while a very low rate constant was found for metallized 7-layers thick multilayer.

The average size of gold nanoparticles in the multilayer is on the order of 3-4 nm. On the other hand, we assume that the thickness of a multilayer is roughly the function of

the amount of the adsorbed DNA having the 2 nm diameter of double helix. From the correlation between the thickness of DNA chain and the average size of gold nanoparticles, and additionally providing that the growth of gold nanoparticles is isotropic and occurs randomly in the vicinity of DNA, we can conclude that the increase of multilayer film thickness leads to (i) the screening of active sites on the surface of catalytic nanoparticles surrounded by polyelectrolytes inside the multilayer, and (ii) the retardation of the diffusion of reactants toward catalytic centers especially located in the inner pare of the multilayer. According to this scenario, the thickness of 7-layers film reaches the value of *ca.* 10 nm, which is significantly larger than the size of embedded NP and steric inhibition becomes important. It should be, however, mentioned, that the construction of PE multilayer does not necessarily result in the tightly packed films, but the effect of film's thickness increase would be the same as described above.

Similarly, the catalytic activity of metallized multilayers prepared form non-saturated by gold multilayers was further investigated and the corresponding kinetic curves are shown in **Figure 7C**. Decrease in the average size of gold NPs inside the multilayer and their surface density was accompanied by a gradual decrease of the catalytic reaction rates, both apparent and surface-normalized (**Table 1**), therefore, the decrease of rate constant was much pronounced to be explained solely by the decreasing of the catalyst's surface area. On the other hand,it is known that electronic properties of gold nanoparticles change significantly for NP sizes smaller than 3 nm, which results in a disappearance of the metallic character of gold clusters and decrease of their catalytic activity.[14, 16] **Table 1** shows that fraction of gold nanoparticles of sizes larger than 3 nm that were synthesized in saturated by gold multilayers is very high, while in the case of undersaturated multilayers the larger part of gold NP size distribution is below 3 nm

and does not contribute to the activity of the catalyst. Therefore, the decrease of the catalytic activity of metallized multilayers synthesized under non-saturated by gold conditions can be rationally explained by the decrease of gold NP size below 3 nm.

The synthesized hybrid catalyst is stable against temperature as well as biological degradation. The increase of solution temperature until 100°C or ultrasound sonication do not induce any release of DNA (<0.1%) from multilayers as was measured by UV spectroscopy of the supernatant above beads. Similarly, addition of DNase enzyme into solution of multilayers and incubation at 36°C under appropriate physiological salt conditions also caused no measurable release of DNA (<0.1%) from multilayers into solution..

4. Conclusion

DNA-based multilayer films can be used as multifunctional matrices for the absorbance of noble metal precursor and its conversion to noble metal nanoparticles. Beads containing metallized multilayers are easily dispersed in solution to provide a good contact of reactants with the catalyst, easily separated after reaction by decantation or filtration, and further reused. The essential advantages of the proposed DNA-based material in comparison to the analogous hitherto reported composite multilayers are (i) the efficient uptake of noble metal from solution resulted in the formation of a stable complex between metal precursor and DNA, and (ii) stabilization of growth of ultrasmall and catalytically active metal nanoparticles of a high density inside the multilayer matrix. The best catalytic performance was found for multilayers containing the minimal number of polyelectrolyte layers apparently due to accessibility of the catalytic nanoparticles.

5. Experimental Section

Materials DNA sodium salt (300 bp in average or 20,000 bp in average) extracted from salmon milt was a gift from Maruha Nichiro Holdings, Inc. (Japan). Poly(diallyldimethylammonium) chloride solution (PDADMAC, M_w = 100,000 – 200,000, 20 wt %), hydrogen tetrachloroaurate $HAuCl_4$ (30 wt % solution in dilute hydrochloric acid, 99.99%), $AgNO_3$ (99.9999%), and sodium borohydride ($NaBH_4$) were from Sigma-Aldrich (USA). Sodium carbonate (Na_2CO_3, 99.8%) was from Kanto Chemical (Japan). Calcium chloride dehydrate ($CaCl_2 \cdot 2H_2O$, 99.0%), sodium acetate (CH_3COONa, 98.5%), sodium chloride (NaCl), sodium hydroxide (NaOH), and p-nitrophenol were from Wako Pure Chemical Industry Co., Ltd (Japan). Acetic acid (CH_3COOH, 99.5%) was from Tokyo Chemical Industries Ltd. (Japan). Disodium dihydrogen ethylendiaminetetraacetate dihydrate (EDTA) and ethanol were from Nacalai Tesque (Japan). Fluorescent dye DAPI (4',6-diamidinio-2-phenyl-indole) was purchased from Wako Pure Chemical Industries, LTD (Japan) and calcein was purchased from Nacalai Tesque, Inc. (Japan). Milli-Q water purified by Simplicity UV apparatus (Millipore, Japan) was used in all experiments.

UV-vis spectroscopy UV-vis spectra of metallized multilayered capsules were recorded on a Jasco V-630 (Japan) spectrophotometer in 1 mL, 1 cm light pass quartz cells at room temperature.

Atomic absorption spectroscopy (AAS) The concentration of Au in solutions was measured on a Hitachi Z-5710 (Japan) atomic absorption spectrometer. Corresponding 1000 ppm standard solution of gold dissolved in concentrated hydrochloric acid was used as a standard for calibration before measurements.

Light and fluorescence microscopy (LM and FM) Light and fluorescence microscopy (FM) observations were performed on an Eclipse TE2000-U microscope (Nikon Instruments Inc.) equipped with an oil-immersed 100x or 40x lens. Digital color pictures were obtained by image-analysis system (Micron Optics, Cedar Knoll, NJ, USA) equipped with a Nikon DS-Ri1 digital camera, and a computer with a NIS-Elements BR 3.1 software.

Transmission Electron Microscopy (TEM) TEM observations and element composition analysis of metallized multilayers were performed at room temperature on a HITACHI H-800 microscope (Japan) equipped with an energy dispersive spectroscopy (EDS) detector at 150-200 kV acceleration voltage. Twenty μL of microcapsules solution was placed onto a 3 mm copper grid covered with a collodion film. After 5 min the solution was removed with a filter paper, and the samples were dried under ambient conditions overnight prior to observations.

Preparation of $CaCO_3$ microparticles Fifty mL of 0.33 M Na_2CO_3 solution were rapidly poured into an equal volume of 0.33 M $CaCl_2$ solution at room temperature. After intense agitation on a magnetic stirrer for 1 min, the precipitate was allowed to settle down, filtered off, and washed once with Milli-Q water and twice with ethanol, and dried at 85 °C in a dry oven for 3 hours. Freshly prepared $CaCO_3$ beads were used for multilayer deposition.

Deposition of DNA-PDADMAC multilayer on $CaCO_3$ template DNA solution was prepared in an acetate buffer (0.01 M, pH = 4.0) by stirring at room temperature over 1 day and the resulted pH of this solution was 4.5. DNA-PDADMAC multilayers were prepared by alternating incubation of $CaCO_3$ microparticles (0.5% w/w in suspension) in DNA (1 g/L) and PDADMAC 1 g/L solution in 0.1 M NaCl each. After each

adsorption cycle performed as 3 min vigorous agitation by vortex, precipitates were washed twice (each for 2 min) with 0.05 M NaCl solution to remove non-bound polyelectrolyte and stored at 4 °C in 0.05 M NaCl solution.

Synthesis of gold and silver nanoparticles inside multilayered microcapsules Beads containing DNA-PDADMAC multilayers (0.5%, 5 mL) were separated by centrifugation (100 *g*, 1 min), supernatant solution was removed and 3 mL solution of 0.6 to 2.9 mM $HAuCl_4$ was added and incubated for 3h. The resulted microbeads were rinsed by 0.05 M NaCl solution, redispersed in 1 mL of Milli-Q water, and 10 μL of 1 M freshly prepared $NaBH_4$ solution was added to induce Au ion reduction. The resulted beads with metallized multilayers were stored in Milli-Q water. Metallization of capsules with silver was performed in a similar manner by saturation of multilayers with $AgNO_3$ and reduction by $NaBH_4$.

Catalytic reduction of p-nitrophenol in the presence of metallized multilayers To 2 mL of 0.02 mM solution of p-nitrophenol in Milli-Q water containing freshly prepared $NaBH_4$ (10 mM), 10 μL of 2.5% microbeads with metallized multilayers were added directly into the spectroscopic cell, and time resolved spectra of the supernatant microbeads were recorded.

Acknowledgements

This work was supported by 25620183 (Grant-in-Aid for Exploratory Research). Maruha Nichiro Holdings, Inc. (Japan) is gratefully acknowledged for free DNA samples extracted from salmon milt. We thank High Voltage Electron Microscope Laboratory at EcoTopia Science Institute, Nagoya University, for the assistance with the TEM observations.

Received: ((will be filled in by the editorial staff))
Revised: ((will be filled in by the editorial staff))
Published online: ((will be filled in by the editorial staff))

References

[1] a) M. C. Daniel, D. Astruc, *Chem Rev* **2004**, *104*, 293-346; b) C. Burda, X. B. Chen, R. Narayanan, M. A. El-Sayed, *Chem Rev* **2005**, *105*, 1025-1102; c) T. K. Sau, C. J. Murphy, *J Am Chem Soc* **2004**, *126*, 8648-8649.

[2] J. Park, J. Joo, S. G. Kwon, Y. Jang, T. Hyeon, *Angew Chem Int Edit* **2007**, *46*, 4630-4660.

[3] a) J. H. Kim, T. R. Lee, *Langmuir* **2007**, *23*, 6504-6509; b) I. Yoon, A. M. Zimmerman, C. C. Tester, A. M. DiCiccio, Y. N. Jiang, W. Chen, *Chem Mater* **2009**, *21*, 3924-3932; c) V. Ramtenki, V. D. Anumon, M. V. Badiger, B. L. V. Prasad, *Colloid Surface A* **2012**, *414*, 296-301; d) C. H. Zhu, Z. B. Hai, C. H. Cui, H. H. Li, J. F. Chen, S. H. Yu, *Small* **2012**, *8*, 930-936; e) M. J. Hortiguela, I. Aranaz, M. C. Gutierrez, M. L. Ferrer, F. del Monte, *Biomacromolecules* **2011**, *12*, 179-186; f) N. Welsch, M. Ballauff, Y. Lu, *Adv Polym Sci* **2010**, *234*, 129-163; g) Y. Lu, P. Spyra, Y. Mei, M. Ballauff, A. Pich, *Macromol Chem Phys* **2007**, *208*, 254-261; h) S. Wunder, F. Polzer, Y. Lu, Y. Mei, M. Ballauff, *J. Phys. Chem. C* **2010**, *114*, 8814; i) S. Wunder, Y. Lu, M. Albrecht, M. Ballauff, *ACS Catal.* **2011**, *1*, 908; j) A. Zinchenko, Y. Miwa, L. I. Lopatina, V. G. Sergeyev, S. Murata, *Acs Appl Mater Inter* **2014**, *6*, 3226-3232.

[4] a) M. L. Bruening, D. M. Dotzauer, P. Jain, L. Ouyang, G. L. Baker, *Langmuir* **2008**, *24*, 7663-7673; b) D. A. Dotzauer, S. Bhattacharjee, Y. Wen, M. L. Bruening, *Langmuir* **2009**, *25*, 1865-1871; c) D. M. Dotzauer, J. H. Dai, L. Sun, M. L. Bruening, *Nano Lett* **2006**, *6*, 2268-2272; d) L. Ouyang, D. M. Dotzauer, S. R. Hogg, J. Macanas, J. F. Lahitte, M. L. Bruening, *Catal Today* **2010**, *156*, 100-106; e) S. Joly, R. Kane, L. Radzilowski, T. Wang, A. Wu, R. E. Cohen, E. L. Thomas, M. F. Rubner, *Langmuir* **2000**, *16*, 1354-1359; f) J. H. Dai, M. L. Bruening, *Nano Lett* **2002**, *2*, 497-501; g) W. Schrof, S. Rozouvan, E. Van Keuren, D. Horn, J. Schmitt, G. Decher, *Adv Mater* **1998**, *10*, 338-341; h) S. Kidambi, J. H. Dai, J. Li, M. L. Bruening, *J Am Chem Soc* **2004**, *126*, 2658-2659; i) S. Bhattacharjee, M. L. Bruening, *Langmuir* **2008**, *24*, 2916-2920;

j) S. Bhattacharjee, D. M. Dotzauer, M. L. Bruening, *J Am Chem Soc* **2009**, *131*, 3601-3610.

[5] Y. Che, A. Zinchenko, S. Murata, *J Colloid Interface Sci* **2015**, *445*, 364-370.

[6] a) I. Sissoeff, J. Grisvard, E. Guille, *Prog Biophys Mol Biol* **1976**, *31*, 165-199; b) J. Anastassopoulou, *J Mol Struct* **2003**, *651*, 19-26; c) Y. Takahashi, X. Châtellier, K. H. Hattori, K. Kato, D. Fortin, *Chemical Geology* **2005**, *219*, 53-67; d) Y. Takahashi, M. Yamamoto, Y. Yamamoto, K. Tanaka, *Geochimica Et Cosmochimica Acta* **2010**, *74*, 5443-5462.

[7] a) T. Takeshima, L. Sun, Y. Wang, Y. Yamada, N. Nishi, T. Yonezawa, B. Fugetsu, *Polym. J. (Tokyo, Jpn.)* **2014**, *46*, 36-41; b) M. Yamada, K. Kato, M. Nomizu, N. Sakairi, K. Ohkawa, H. Yamamoto, N. Nishi, *Chem-Eur J* **2002**, *8*, 1407-1412; c) M. Yamada, M. Yokota, M. Kaya, S. Satoh, B. Jonganurakkun, M. Nomizu, N. Nishi, *Polymer* **2005**, *46*, 10102-10112; d) K. Iwata, T. Sawadaishi, S. Nishimura, S. Tokura, N. Nishi, *Int J Biol Macromol* **1996**, *18*, 149-150.

[8] Y. Miwa, A. Zinchenko, L. I. Lopatina, V. G. Sergeyev, S. Murata, *Polym Int* **2014**, *63*, 1566-1571.

[9] a) G. Decher, J. D. Hong, *Makromol Chem-M Symp* **1991**, *46*, 321-327; b) G. Decher, *Layered nanoarchitectures via directed assembly of anionic and cationic molecules*, Pergamon Press, Oxford, **1996**.

[10] D. V. Volodkin, A. I. Petrov, M. Prevot, G. B. Sukhorukov, *Langmuir* **2004**, *20*, 3398-3406.

[11] D. V. Volodkin, N. I. Larionova, G. B. Sukhorukov, *Biomacromolecules* **2004**, *5*, 1962-1972.

[12] S. Wang, K. Qian, X. Z. Bi, W. X. Huang, *J. Phys. Chem. C* **2009**, *113*, 6505-6510.

[13] a) C. K. S. Pillai, U. S. Nandi, *Biopolymers* **1973**, *12*, 1431-1435; b) C. K. S. Pillai, U. S. Nandi, *Biochim Biophys Acta* **1977**, *474*, 11-16.

[14] a) T. Kiyonaga, Q. L. Jin, H. Kobayashi, H. Tada, *Chemphyschem* **2009**, *10*, 2935-2938; b) S. Panigrahi, S. Basu, S. Praharaj, S. Pande, S. Jana, A. Pal, S. K. Ghosh, T. Pal, *J Phys Chem C* **2007**, *111*, 4596-4605; c) C. Lin, K. Tao, D. Y. Hua, Z. Ma, S. H. Zhou, *Molecules* **2013**, *18*, 12609-12620.

[15] Y. Mei, G. Sharma, Y. Lu, M. Ballauff, M. Drechsler, T. Irrgang, R. Kempe, *Langmuir* **2005**, *21*, 12229-12234.

[16] a) I. Laoufi, M. C. Saint-Lager, R. Lazzari, J. Jupille, O. Robach, S. Garaudee, G. Cabailh, P. Dolle, H. Cruguel, A. Bailly, *J Phys Chem C* **2011**, *115*, 4673-4679;

b) M. Valden, X. Lai, D. W. Goodman, *Science* **1998**, *281*, 1647-1650; c) H. Tsunoyama, N. Ichikuni, H. Sakurai, T. Tsukuda, *J Am Chem Soc* **2009**, *131*, 7086-7093; d) H. Tsunoyama, H. Sakurai, T. Tsukuda, *Chem Phys Lett* **2006**, *429*, 528-532.

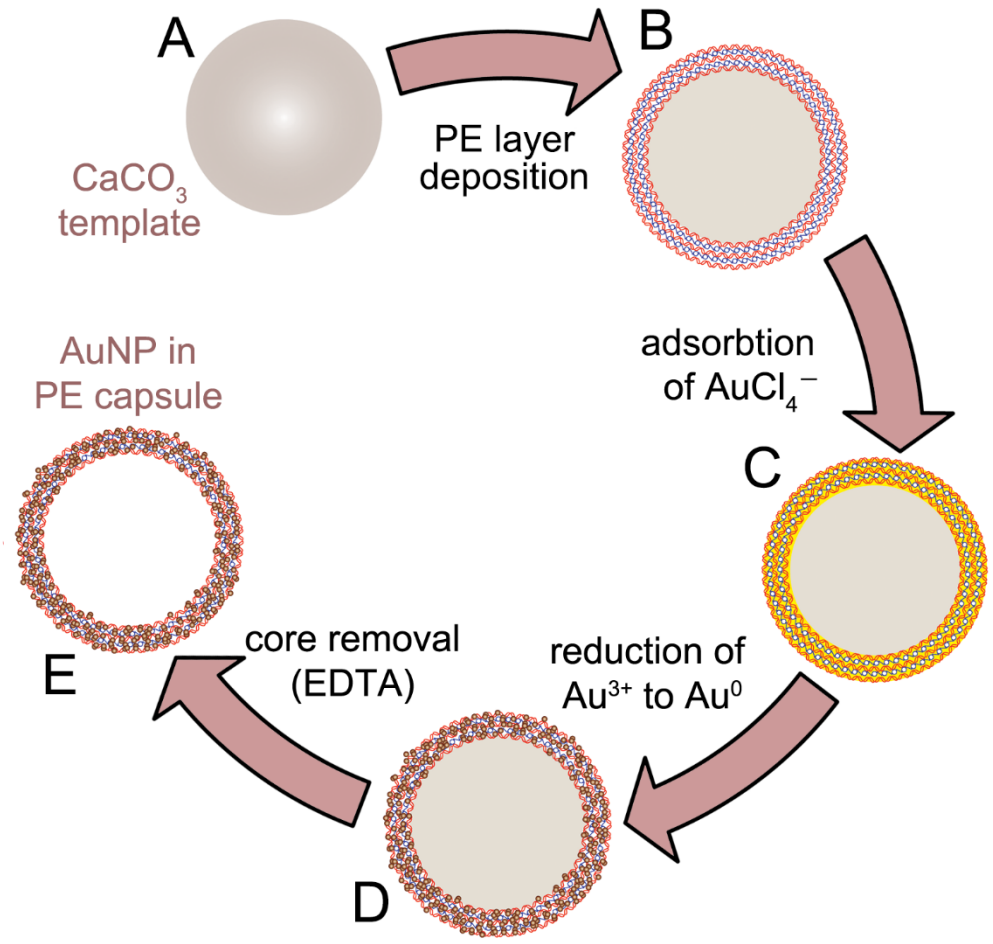

Figure 1. General schematics illustrating the construction of metallized multilayers and their metallization. Deposition of polyelectrolyte multilayer on a surface of $CaCO_3$ template (**A**, **B**), absorption of gold precursor ($HAuCl_4$) by DNA in multilayer film (**C**), metallization of the multilayer by reduction of adsorbed gold ion (**D**), and removal of the sacrificial $CaCO_3$ template by EDTA (**E**).

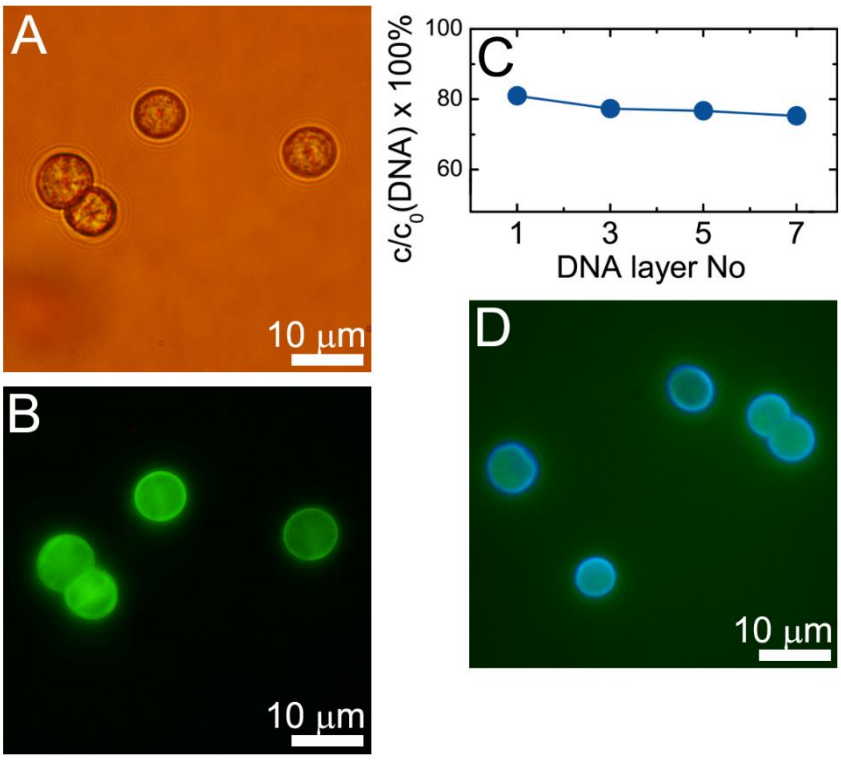

Figure 2. Preparation of $CaCO_3$ microbeads and deposition of DNA-PDADMAC multilayer on bead's surface. A. Optical microscopy image of $CaCO_3$ microbeads. **B.** Fluorescent microscopy image of $CaCO_3$ microbeads stained with Ca^{2+} selective fluorescent dye, calcein. **C.** The percentage of the remained DNA in 1 g/L DNA solutions after deposition of 1^{st}, 3^{rd}, 5^{th}, and 7^{th} layers of DNA on 0.5 % (w/w) $CaCO_3$ beads. The data were obtained from the absorbance spectra of DNA in a supernatant at 260 nm. **D.** Typical fluorescent microscopy images of $CaCO_3$ beads with deposited polyelectrolyte multilayer ($(DNA)_3(PDADMAC)_2$) stained by DNA-specific DAPI fluorescent probe (blue) and by Ca^{2+} specific calcein florescent probe (green).

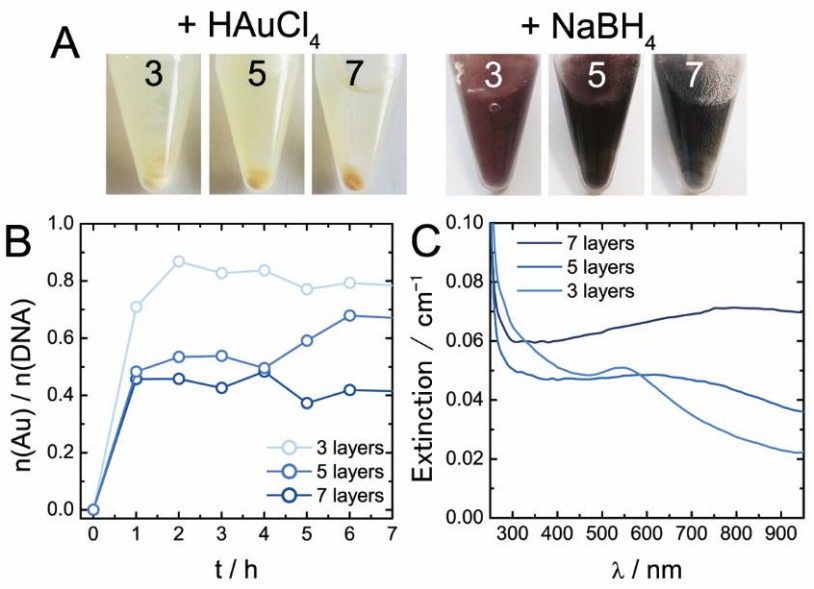

Figure 3. Metallization of beads with DNA-PDADMAC multilayers and their optical properties. **A**. Photographic images of $(DNA)_2(PDADMAC)_1$, $(DNA)_3(PDADMAC)_2$, and $(DNA)_4(PDADMAC)_3$ beads (2.5%) containing 3, 5, and 7 polyelectrolyte layers after saturation with $HAuCl_4$ (left), and sequential reduction by $NaBH_4$ (right). (**B**) Time-dependent $HAuCl_4$ uptake by beads (0.5%) from 1 mL solution containing 2.9 mM $HAuCl_4$ shown as a molar ratio of absorbed Au ions to DNA phosphate groups. The molar ratios were calculated based on the amount of DNA deposited on beads measured by UV-Vis spectroscopy and the amount of adsorbed gold measured by atomic adsorption spectroscopy. (**C**) Extinction (the sum of scattering and absorption) spectra of $(DNA)_2(PDADMAC)_1$, $(DNA)_3(PDADMAC)_2$, and $(DNA)_4(PDADMAC)_3$ capsules (0.25%) containing 3, 5, and 7 layers after metallization.

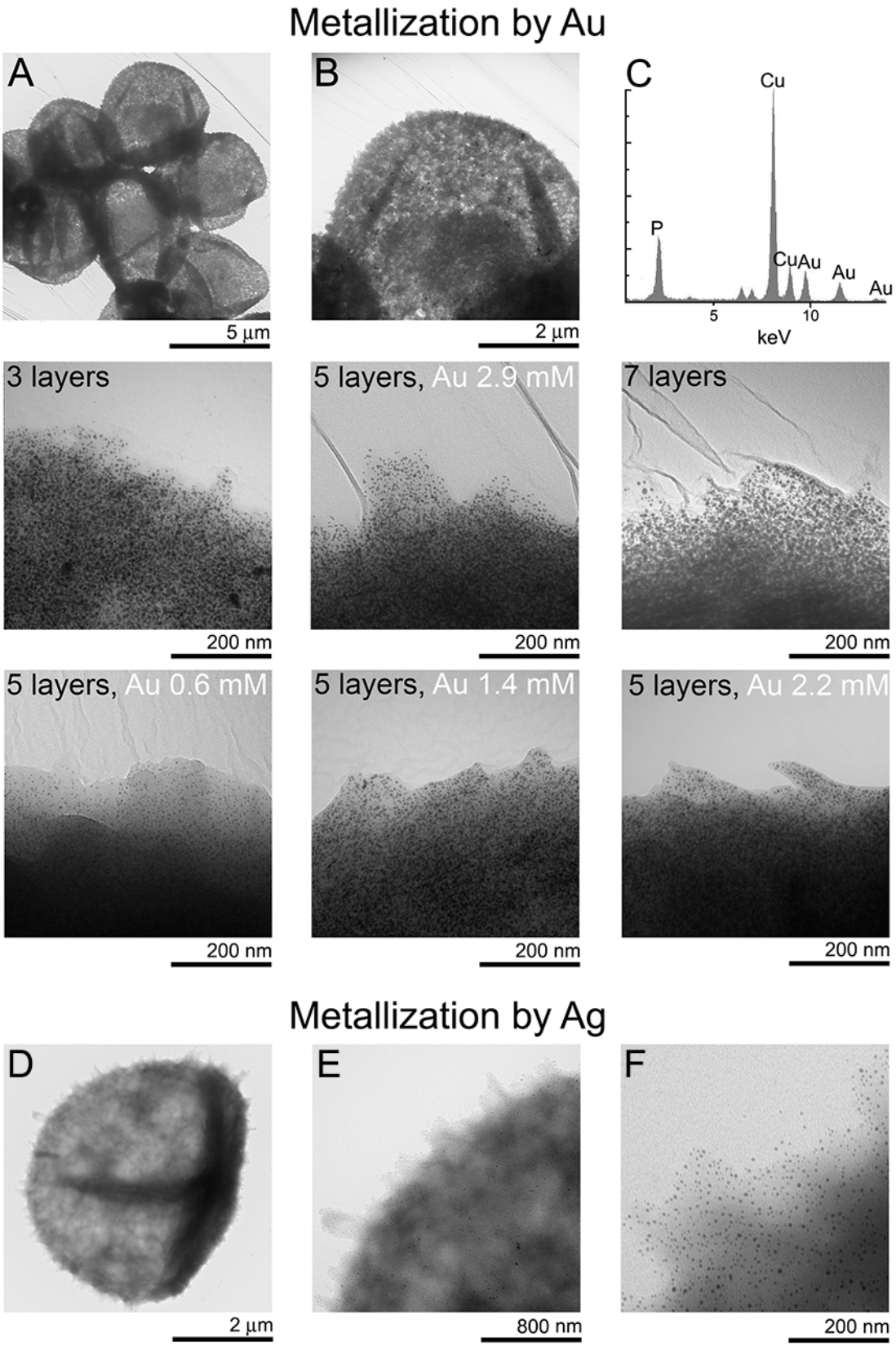
Metallization by Au
A
5 µm
B
2 µm
C
Cu
P
CuAu
Au
Au
5
10
keV
3 layers
200 nm
5 layers, Au 2.9 mM
200 nm
7 layers
200 nm
5 layers, Au 0.6 mM
200 nm
5 layers, Au 1.4 mM
200 nm
5 layers, Au 2.2 mM
200 nm
Metallization by Ag
D
2 µm
E
800 nm
F
200 nm

Figure 4. Transmission electron microscopy analysis of NP embedded in DNA-PDADMAC capsules. (**A-B**) TEM images of the typical $(DNA)_3(PDADMAC)_2$ capsules after metallization with gold. (**C**) EDS spectra of $(DNA)_3(PDADMAC)_2$ capsule fragment (spot size 200 nm) after metallization with gold. The signal of Cu is from the microscopic grid. (**Middle**) Typical TEM images of metallized multilayers containing different number of layers (3 layers - $(DNA)_2(PDADMAC)_1$, 5 layers - $(DNA)_3(PDADMAC)_2$, and 7 layers - $(DNA)_4(PDADMAC)_3$) and different amount of adsorbed gold before metallization. The number of layers and concentration of $HAuCl_4$ solution used of gold adsorption are indicated on the corresponding images. (High resolutions images of metallized multilayers are available online as Supporting Information) (**D-F**) TEM images of a typical $(DNA)_3(PDADMAC)_2$ capsule and multilayer after metallization with sliver.

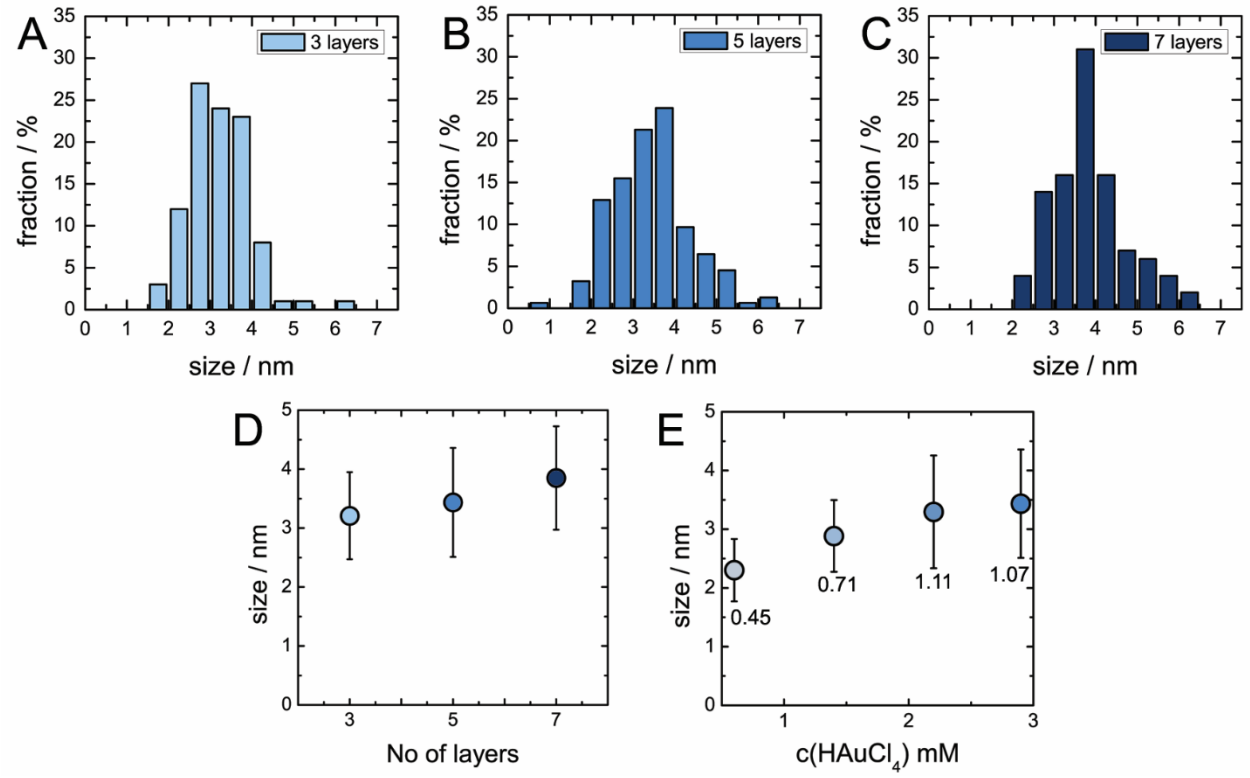

Figure 5. Size distributions of gold nanoparticles. (**A-C**) Size distributions of gold nanoparticles synthesized in $(DNA)_2(PDADMAC)_1$ (**A**), $(DNA)_3(PDADMAC)_2$ (**B**), and $(DNA)_4(PDADMAC)_3$ (**C**) multilayers. (**D**) Dependence of the average size of gold nanoparticles synthesized in multilayers on the number of layers. (**E**) Dependence of the average size of gold nanoparticles synthesized in $(DNA)_3(PDADMAC)_2$ on the concentration of $HAuCl_4$ in solution used for saturation of multilayers with gold. The conditions of the highest concentration (2.9 mM) correspond to the saturation of DNA in multilayers with gold. Values above experimental points indicate the Au/P ratios in metallized multilayers measured by EDS. Analysis of gold nanoparticles size was performed by measuring at least 100 NP. The error bars in plots **D** and **E** show statistical deviations from the mean values.

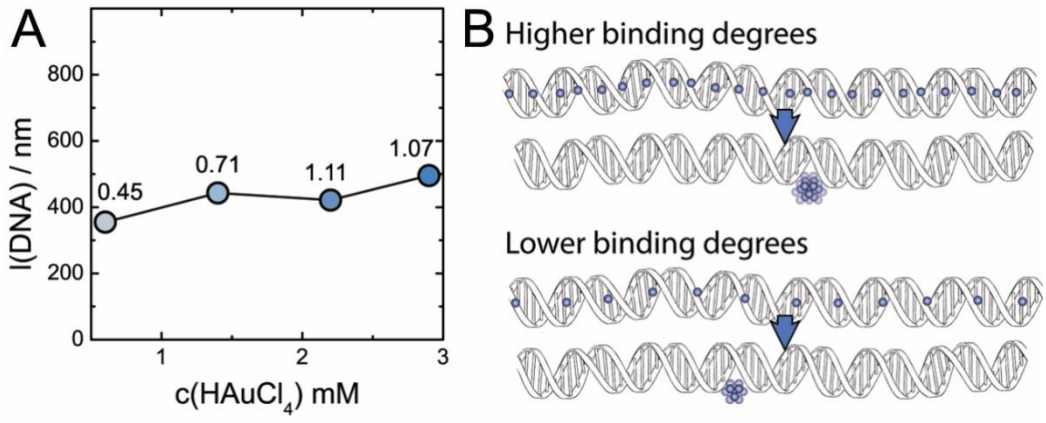

Figure 6. A model of NP growth on DNA template. (**A**) Dependence of the average DNA length corresponding to number of Au atoms used to construct one gold nanoparticle in $(DNA)_3(PDADMAC)_2$ multilayer at different Au/DNA ratios shown above experimental points. The conditions with the highest concentration (2.9 mM) correspond to saturation of DNA in multilayers with gold. Values above experimental points indicate Au/P ratios measured by EDS. (**B**) The schematics illustrating the proposed model of gold NP formation at different degrees of DNA saturation with gold..

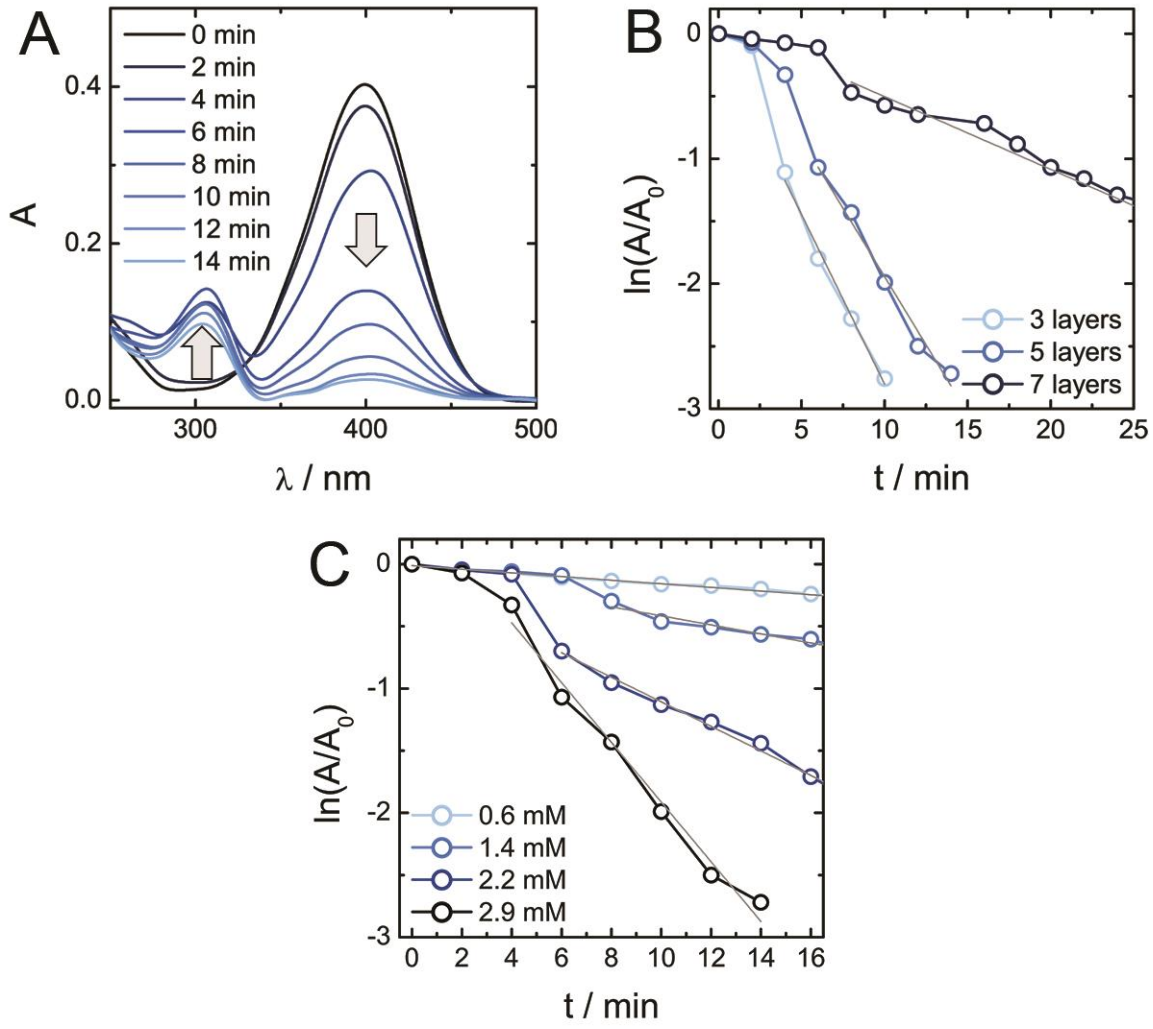

Figure 7. Catalysis by gold nanoparticles embedded into DNA-PDADMAC multilayers. (**A**) Time dependent changes in UV-vis absorbance spectra of solution containing 0.02 mM *p*-nitrophenol 10 mM $NaBH_4$ 0.1 g of metallized beads with $(DNA)_3(PDADMAC)_2$ multilayer after addition of. (**B**) Time dependence of the normalized nitrophenol absorbance at λ= 400 nm in solutions containing the same concentration of $(DNA)_2(PDADMAC)_1$, $(DNA)_3(PDADMAC)_2$, and $(DNA)_4(PDADMAC)_3$. (**C**) Time dependence of the normalized nitrophenol absorbance at λ= 400 nm in solutions containing the same concentrations of $(DNA)_3(PDADMAC)_2$ metallized by different amounts of gold.

Table 1. Characteristics of various multilayers prepared in this study: Au/P ratios in the metallized multilayers measured by EDS, the average size of Au nanoparticles formed in the multilayers, apparent (k_{app}) and surface-normalized (k_1) kinetic constants of p-nitrophenol reduction performed under identical conditions.

Type of multilayers	Au/P (EDS)	NP size / nm	k_{app} / s^{-1}	k_1 / s^{-1} m^{-2} l
$(DNA)_2(PDADMAC)_1$	1.46	3.20 ± 0.73	2.79×10^{-1}	8.19×10^{-1}
$(DNA)_3(PDADMAC)_2$	1.07	3.76 ± 0.77	2.40×10^{-1}	6.89×10^{-1}
$(DNA)_4(PDADMAC)_3$	1.29	3.85 ± 0.88	5.82×10^{-2}	1.06×10^{-1}
$(DNA)_3(PDADMAC)_2$	0.45	2.31 ± 0.47	1.46×10^{-2}	6.48×10^{-1}
	0.71	2.91 ± 0.55	3.63×10^{-2}	1.22×10^{-1}
	1.11	3.29 ± 0.85	9.86×10^{-2}	2.39×10^{-1}
	1.07 (sat.)	3.76 ± 0.77	2.40×10^{-1}	6.89×10^{-1}

DNA-containing polyelectrolyte multilayers was utilized as a host matrix for synthesis and size control of ultra-small gold nanoparticles. The resulted thin films with embedded gold NP are promising hybrid materials for catalytic applications. The catalytic activity of gold NP was shown to depend on the structure of the host multilayer.

Keywords DNA, multilayers, gold nanoparticles, size control, catalysis

Anatoly Zinchenko,* Chihiro Nagahama, Shizuaki Murata

Gold Nanoparticles in DNA-Based Multilayer Films: Synthesis, Size Control, and Influence of the Multilayer Structure on Au NP Catalytic Properties